Pergamon

0301-9322(94)00095-6

Int. J. Multiphase Flow Vol. 21, No. 4, pp. 545–560, 1995

0301-9322/95 $9.50 + 0.00

DROP DEFORMATION AND BREAKUP DUE TO SHOCK WAVE AND STEADY DISTURBANCES

L.-P. HSIANG and G. M. FAETH†

Department of Aerospace Engineering, The University of Michigan, Ann Arbor, MI 48109-2118, U.S.A.

(Received 17 May 1994; in revised form 19 December 1994)

Abstract—An experimental study of drop deformation properties induced by both shock wave and steady disturbances is described. Three test facilities were used, as follows: a shock tube facility for measurements of effects of shock wave disturbances on drops in gases, a 10 m high drop tube facility for measurements of effects of steady disturbances on drops in gases and a 1 m high drop tube facility for measurements of effects of steady disturbances on drops in liquids. Various dispersed and continuous phase gases and liquids were considered to provide dispersed/continuous phase density ratios of 1.15–12,000, Ohnesorge numbers of 0.0006–600, Weber numbers of 0.004–700 and Reynolds numbers of 0.03–16,000. At low Ohnesorge numbers (<0.1) for all types of disturbances, significant drop deformation (5%) began at Weber numbers of roughly unity, with the deformation regime ending due to the onset of breakup at Weber numbers of 10–20. These transitions were relatively unaffected by the Ohnesorge number for steady disturbances, however, increasing Ohnesorge numbers caused progressive increases of the Weber number range for both deformation and breakup regimes for shock wave disturbances—an effect that could be explained using phenomenological theory. Another transition, between dome- and bowl-shaped drops (related to the transition between bag and shear breakup), was correlated mainly in terms of Weber and Reynolds numbers for present conditions. Drop deformation for steady disturbances was relatively independent of dispersed/continuous phase density ratios but generally was smaller than for shock wave disturbances at comparable conditions due to the absence of overshoot from inertial effects. In contrast, drop drag coefficients, normalized by the drag coefficient of a solid sphere at the same Reynolds number, were correlated quite well by the degree of deformation alone.

Key Words: drop deformation, drop dynamics, drop breakup, atomization, pulsed holography

1. INTRODUCTION

Processes of deformation and secondary breakup of drops have received significant attention as important classical multiphase flow phenomena with numerous practical applications, e.g. industrial and agricultural sprays, liquid-fueled power and propulsion systems, and rainfall, among others. In particular, recent studies suggest that secondary breakup is a rate-controlling process in the near-injector region of pressure-atomized sprays, through its effect on drop sizes (Ruff *et al.* 1992). Additionally, primary breakup at the surface of non-turbulent and turbulent liquids yields drops that intrinsically are unstable to secondary breakup (Wu *et al.* 1991, 1992), supporting the classical description that atomization occurs by primary breakup near a liquid surface followed by secondary breakup (Faeth 1990). Finally high pressure combustion involves conditions where the drop surface tension becomes small because the liquid surface approaches the thermodynamic critical point: such conditions also imply significant effects of secondary drop deformation and breakup. Motivated by these observations, the objectives of the present investigation were to extend earlier studies of secondary drop deformation and breakup in this laboratory, due to Hsiang & Faeth (1992, 1993), emphasizing the properties of drop deformation from both shock wave and continuous disturbances.

Past work on drop deformation and breakup will only be considered briefly [see Wierzba & Takayama (1987), Giffen & Muraszew (1953), Hinze (1955), Krzeczkowski (1980), Clift *et al.* (1978) and references cited therein, for more complete reviews]. Past work generally has been limited to two kinds of well-defined disturbances that cause deformation and breakup of drops: shock wave disturbances that provide step changes in the ambient environment of a drop, e.g. representing a

†To whom correspondence should be addressed.

drop at the end of rapid primary breakup; and steady disturbances, e.g representing freely-falling drops in a rainstorm or a mixing column. Effects of shock wave disturbances have received the most attention with high-speed photography used to identify deformation and secondary breakup regimes. Measurements of transitions between breakup regimes have been limited to dispersed/continuous-phase density ratios, $\rho_d/\rho_c > 500$ and Reynolds numbers, $\mathrm{Re} = \rho\, d_o u_o/\mu_c > 500$, where d_o and u_o denote the original drop diameter and relative velocity and μ_c is the continuous-phase viscosity. For these conditions, Hinze (1955) shows that breakup regime transitions largely are functions of the ratio of drag to surface tension forces, represented by the Weber number, $\mathrm{We} = \rho_c d_o u_o^2/\sigma$, and the ratio of liquid viscous to surface tension forces, represented by the Ohnesorge number, $\mathrm{Oh} = \mu_d/(\rho_d d_o \sigma)^{1/2}$, where σ is the surface tension and μ_d is the dispersed-phase viscosity. At low Oh, drop deformation becomes significant at We of roughly 1 and drop breakup becomes significant at We of roughly 10, with bag, multimode and shear breakup regimes observed at progressively larger We [see Wierzba & Takayama (1987), Giffen & Muraszew (1953), Hinze (1955), Krzeckowski (1980) and Clift *et al.* (1978) for photographs and detailed descriptions of the various types of drop breakup]. With increasing Oh, however, progressively larger We are required for the onset of drop deformation and breakup because viscous forces inhibit drop deformation which is the first stage of the breakup process. This behavior has been confirmed by several investigations, however, maximum values of $\mathrm{Oh} < 4$ so that behavior at large Oh has not been resolved. This is unfortunate because high pressure combustion processes involve large Oh as a result of drop surfaces approaching the thermodynamic critical point. This behavior occurs because surface tension becomes small while liquid viscosity remains finite as liquid surfaces approach their thermodynamic critical point (Faeth 1990). Thus, whether combustion at high pressures involves enhanced, or entirely suppressed, effects of secondary breakup has not yet been resolved.

The time required for breakup is another aspect of secondary breakup that has received significant attention for shock wave disturbances at $\rho_d/\rho_c > 500$. At low Oh, Liang *et al.* (1988) found that breakup times normalized by the characteristic breakup time of Ranger & Nicholls (1969), $t^* = d_o(\rho_d/\rho_c)^{1/2}/u_o$, were remarkably independent of both the breakup regime and We. As might be expected from the effect of Oh on breakup regimes, however, breakup times have been observed to increase with increasing Oh (Hsiang & Faeth 1992). Additionally, processes of drop deformation, and the variation of drop drag coefficient with time, also appear to scale systematically in terms of t^* at low Oh but behavior at large Oh is uncertain.

Finally, the outcome of secondary breakup for shock wave disturbances at $\rho_d/\rho_c > 500$ and small Oh also has received attention (Hsiang & Faeth 1993; Gel'fand *et al.* 1974). It was found that drop size distributions after secondary breakup satisfied the universal root normal distribution of Simmons (1977) in all three breakup regimes, after removing the core (or drop forming) drop from the drop population for shear breakup. The size and velocity of the core drop after shear breakup then was correlated successfully based on the observation that the end of drop stripping corresponded to a constant Eötvös number, $\mathrm{Eo} = a\rho_d d_o^2/\sigma$ where a = drop acceleration (Hsiang & Faeth 1993). The relative velocities of the drop liquid were significantly reduced after secondary breakup, which could be correlated successfully based on simplified phenomenological theory (Hsiang & Faeth 1993). These results showed that secondary breakup processes extend over a significant region, roughly 40 initial drop diameters. Thus, secondary breakup is not a particularly localized event which raises concerns about its dynamics, e.g. liquid motion during breakup, the distribution of drop liquid in space and time, etc. Work treating these issues, however, has not yet been reported.

Drop deformation and breakup for steady disturbances also has been studied, motivated by interest in the properties of rain and liquid–liquid extraction equipment. The main objective of this work has been to develop ways to estimate the velocity of fall of particular sized drops in gas and liquid environments, and to determine conditions for drop breakup. It has been found that We for breakup are comparable for steady and shock wave disturbances. However, the properties of breakup for steady disturbances are not well understood due to the intrusion of processes of drop formation. For example, whether the mechanism of breakup is due to nozzle-induced disturbances, bag breakup, simple splitting into a few drops or is significantly affected by collisions, still has not been resolved (Pruppacher & Pitter 1971; Ryan 1976). Other areas of uncertainty involve relationships between drop deformation and drag, effects of large Oh and the relationships between

the parameters of dispersed and continuous phases and the drop shape. Since steady disturbances provide conditions where drop deformation and breakup response to disturbance levels are relatively simple to interpret and to correlate, it is clear that more progress on effects of steady disturbances must be made before the more complex processes involving shock wave or more general disturbances can be understood.

The objective of the present investigation was to extend the work of Hsiang & Faeth (1992, 1993) in order to help resolve some of the issues discussed in the preceding review of the literature. Foremost among these issues is the nature of the deformation and breakup regime map for shock wave disturbances at large Oh. Other issues considered involved factors influencing drop deformation and shape, emphasizing effects of the dispersed/continuous phase density ratio, and the relationship between drop drag and deformation in various environments. These problems were addressed using three test facilities, as follows: a shock tube facility for measurements of effects of shock wave disturbances on drops in gases, a 10 m high drop tube facility for measurements of effects of steady disturbances on drops in gases, and a 1 m high drop tube facility for measurements of effects of steady disturbances on drops in liquids. Various dispersed and continuous phase gases and liquids were used to provide ρ_d/ρ_c of 1.15–12,000, Oh of 0.0005–600, We of 0.004–700 and Re of 0.03–16,000. Phenomenological analysis was used to help interpret and correlate some aspects of the measurements.

The paper begins with a discussion of experimental methods. Results are then considered, treating drop deformation and breakup regimes, drop deformation and drop drag, in turn.

2. EXPERIMENTAL METHODS

2.1. Shock tube

Apparatus. The shock tube apparatus involved a driven section open to the atmosphere, similar to earlier work in this laboratory (Hsiang & Faeth 1992, 1993). The driven section had a rectangular cross section (38 mm wide × 64 mm high) and a length of 6.7 m with the test location 4.0 m from the downstream end. This provided test times of 17–21 ms in the uniform flow region behind the incident shock wave. In particular, worst-case variations of continuous phase properties during breakup processes were less than 5%. The test location had quartz windows (25 mm high × 305 mm long, mounted flush with the interior side walls of the shock tube) to allow observation of drop breakup. Breakup was observed in air initially at 98 kPa and 297 ± 2 K in the driven section of the shock tube with shock Mach numbers in the range 1.08–1.31. Instrumentation was synchronized with the passing of the shock wave using the piezoelectric pressure transducers that monitored the strength of the shock wave in the driven section.

Two different drop generator systems were used for the shock tube experiments. Operation at low and moderate Oh involved the use of a vibrating capillary tube drop generator, similar to Dabora (1967), which generated a stream of drops. This drop stream passed through 6 mm diameter holes in the top and bottom of the shock tube, crossing the central plane of the driven section at the test location. An electrostatic drop selection system, similar to Sanjiovanni & Kestin (1977), was used to deflect a fraction of the drops out of the stream. This yielded a drop spacing of roughly 7 mm so that drops were always present in the region observed while interactions between drops during secondary breakup were eliminated.

Drop generation for large Oh conditions required a different approach. In particular, it is very difficult to form a drop that has a large Oh; instead, such drops generally evolve to these conditions after formation at low Oh, e.g. large Oh conditions are approached during high pressure combustion because the drop surface eventually becomes heated to conditions near the thermodynamic critical point. The approach taken during the present investigation was to form a low Oh drop from a liquid solution, and to levitate the drop at the test location until the solvent evaporated away, leaving a small drop consisting of a highly viscous liquid which provided the desired large Oh condition. Dow Corning 200 Fluids having unusually large viscosities (10,000 and 30,000 mP) were used for the viscous liquids, with *n*-heptane used as the volatile solvent. Original drop diameters were in the range 320–700 μm, with final drop diameters of 160–350 μm, which required several minutes to complete evaporation of the solvent.

The levitation system consisted of a horn and reflector having diameters of 10 mm that were positioned near the top and bottom of the test section (roughly 55 mm apart). Two 50 mm diameter piezoelectric ceramic elements, combined with a central mount and a resonator, were used to power the horn. The horn operated at a frequency of roughly 47 kHz with the tip of the horn having an amplitude of roughly 200 μm. The piezoelectric ceramic elements were actuated using a Wilcoxan, Model PA8-1 power supply (110 V, 8 A maximum output conditions) operating at the required frequency. A step up transformer was used to increase the output voltage to 1000 V in order to properly drive the ceramic elements. This circuit also incorporated proper impedance matching circuitry for the ceramic elements. The horn driving unit was cooled with an air blower system. The long shank of the horn also helped to minimize thermal disturbances, due to the large power dissipation of the horn driving unit, within the test section. The drops were placed in the acoustic field of the horn and reflector system using a hypodermic syringe. Access to the test section for the syringe was provided by a port that could be sealed by a cap screw, whose inner end was flush with the inside wall of the test section.

Instrumentation. The deformation and breakup process was observed using pulsed shadowgraph motion pictures, similar to earlier work (Hsiang & Faeth 1992, 1993). A copper vapor laser was used as the light source with a 35 mm drum camera used to record the shadowgraph images at unity magnification. A function generator was used to pulse the laser when the shock wave neared the drop stream location, with pulse frequencies of 6–8 kHz for 20 pulses. Each laser pulse duration was 30 ns, which was sufficient to stop the motion of the drop on the rotating film drum. The drum camera recorded the images with an open shutter within a darkened room. The time between shadowgraph pictures was monitored by recording the signal generator output using a digital oscilloscope.

The film records were analyzed using a Gould FD 5000 Image Display. The procedure was to obtain three motion picture shadowgraphs for a particular test condition and group the data to obtain statistically-significant results as ensemble averages. Experimental uncertainties (95% confidence) of the measurements reported here are as follows: relative velocities, less than 10%; initial drop diameter and subsequent drop dimensions, less than 10%; and drop drag coefficients, less than 30%, limited by the accuracy of finding drop centroid motion at small times after passage of the shock wave. Corresponding uncertainties of parameters reported here will be presented when the parameters are discussed.

Test conditions. Test conditions are summarized in table 1. Including results of earlier work (Hsiang & Faeth 1992), test drops of water, *n*-heptane, mercury, two Dow Corning 200 Fluids and various glycerol mixtures were used to provide a wide range of liquid properties. The liquid properties listed in table 1 were obtained from Lange (1952), except for the properties of the Dow Corning 200 Fluids which were obtained from the manufacturer, and the surface tensions of the glycerol mixtures which were measured in the same manner as Wu *et al.* (1991). Initial drop diameters were in the range 150–1550 μm. Ranges of other variables are as follows: ρ_d/ρ_c of 500–12,000, Oh of 0.0006–560, We of 0.5–680 and Re of 340–15,760. The We range includes

Table 1. Summary of liquid–air shock tube test conditions†

Dispersed phase	ρ_d (kg/m^3)	$\mu_d \times 10^4$ (kg/ms)	$\sigma \times 10^3$ (N/m)	d_o (mm)	We	Oh	Re
Water	997	8.94	70.8	1.0	0.5–236	0.0038	340–8250
n-Heptane	683	3.94	20.0	0.5	14–137	0.0036	720–2270
Mercury	13,600	15.0	475.0	0.85	10–13	0.00062	3510–4500
DC200 Fluid‡	980	100,000	20.0	0.15–0.35	35–100	120–185	980–1700
DC200 Fluid‡	980	300,000	20.0	0.15–0.35	100–680	365–555	1170–5200
Glycerol 21%	1050	16.0	67.3	1.2	8–130	0.0071	1540–6390
Glycerol 63%	1162	108.0	64.8	1.2	1–129	0.0390	480–6420
Glycerol 75%	1195	356.0	63.8	1.2	2–128	0.0990	730–6270
Glycerol 84%	1219	1000	63.2	1.2	1–127	0.260	500–6210
Glycerol 92%	1240	3270	62.5	1.2	1–268	1.050	530–8330
Glycerol 97%	1253	8350	62.4	1.5	1–205	1.700	600–8880
Glycerol 99.5%	1260	12,500	62.0	1.55	1–612	3.850	630–15760

†Air initially at 98.8 kPa and 298 ± 3 K in a driven section of shock tube with shock Mach numbers in the range 1.01–1.24.
Properties of air taken at normal temperature and pressure: $\rho_c = 1.18$ kg/m^3, $\mu_c = 18.5 \times 10^{-6}$ kg/m s.
‡Dow Corning 200 fluid.

processes from no deformation into the shear breakup regime of interest to phenomena within dense sprays (Faeth 1990), but does not reach the catastrophic breakup regime studied by Reinecke *et al.* (1969, 1970). The Re range of these measurements is higher than conditions where gas viscosity plays a strong role in drop drag properties; within the present Reynolds number range, the drag coefficient for spheres only varies in the range 0.6–0.4 (Faeth 1990; White 1974). The shock waves were weak to modest so that the physical properties of the gas were essentially the same as room temperature air.

2.2. Drop towers

Apparatus. Gas–liquid and liquid–liquid drop towers were used for tests with steady disturbances. The gas-liquid drop tower was constructed of PVC pipe having an inside diameter of 300 mm and a height of 9.2 m, that was open at the top and the bottom. Drops were released along the axis of the tube, at its top, using a simple buret system. The drops were widely spaced, and reached terminal velocities at roughly 5 m, well before the tube exit. Measurements were made when the drops were roughly 200 mm below the bottom of the tube. Instrumentation was synchronized with the passing of the drop using a simple light interception triggering system based on a HeNe laser directed across the exit of the PVC pipe. Drops were collected in a flask at the end of their fall.

The liquid–liquid drop tower was constructed of Plexiglas to provide a 150×150 mm cross section and a vertical height of 1.2 m. The dispersed (drop) and continuous phase liquids were immiscible, and were fully saturated with the other liquid prior to testing. The drop liquid was released using a buret discharging under the surface of the continuous phase liquid. The method of drop introduction was not important for present results, however, because terminal velocity conditions were reached well before the region where measurements were made. Present test conditions did not involve oscillating drops. Measurements were made roughly 300 mm above the bottom of the tank. Drop motion for these conditions was very slow so that it was possible to use manual synchronization when obtaining test records. Drops simply collected at the bottom of the drop tower as an immiscible liquid layer that was removed from time to time.

Instrumentation. Drops were observed using single- and double-pulsed shadowgraph photographs. The light source was a General Radio lamp (type U-31A) with a flash duration of roughly 1 μs. The lamp output was collimated and directed horizontally through the axis of the drop tower. The image was recorded using a Graphlex camera (4×5 in. film format, Polaroid Type 55 film) at a magnification of 6:1. The photographs were obtained in a darkened room using an open camera shutter. The time of separation between pulses was controlled by a function generator. As noted earlier, the time of the first photograph was controlled by a light interception system for the liquid–gas experiments, and manually for the liquid–liquid experiments. These images were processed similar to the shock tube measurements. Experimental uncertainties (95% confidence) of the measurements reported here are as follows: drop velocities, less than 5%; drop dimensions, less than 5%; and drop drag coefficient, less than 10%. The latter two uncertainties were dominated by finite sampling accuracy. As before, corresponding uncertainties of parameters reported here will be presented when the parameters are discussed.

The effective diameters of the drops were computed similar to earlier work (Hsiang & Faeth 1992, 1993). This involved measuring maximum and minimum diameters through the centroid of the image; d_{max} and d_{min}. Assuming ellipsoidal shapes, the diameter was then taken to be the diameter of a sphere having the same volume; namely, $d^3 = d_{min}^2 d_{max}$.

Test conditions. Test conditions for drops falling at their terminal velocities in air are summarized in table 2. In this case, test liquids were limited to water and various glycerol mixtures, with properties found as described for table 1. Initial drop diameters were in the range 2.0–7.8 mm while the ranges of other variables were as follows: ρ_d/ρ_c of 845–1070, Oh of 0.0012–2.9, We of 1.2–9.8 and Re of 830–4600. In this case, the range of We was rather narrow because smaller values resulted in negligible drop deformation, while larger values caused drop breakup, over the available range of Oh. Similar to the test conditions of table 1, the present Reynolds number range involves a rather modest variation of drop drag coefficients.

Test conditions for the liquid–liquid drop tower experiments are summarized in table 3. Test liquids for the dispersed phase included water, ethylene glycol, various glycerol mixtures, carbon disulfide and a Dow Corning 200 Fluid having a viscosity of 30,000 cP. Test liquids for the

Table 2. Summary of liquid–air drop tower test conditions†

Dispersed phase	ρ_d (kg/m^3)	$\mu_d \times 10^4$ (kg/ms)	$\sigma \times 10^3$ (N/m)	d_o (mm)	We	Oh	Re
Water	997	8.94	70.8	2.0–7.8	1.2–9.8	0.0012–0.0024	830–46000
Glycerol 42%	1105	35.0	65.4	2.0–7.8	1.4–9.5	0.0046–0.0091	870–4210
Glycerol 63%	1162	108.0	64.8	2.0–7.8	1.5–9.8	0.0140–0.0275	880–4390
Glycerol 84%	1219	1000	63.2	2.0–7.8	1.7–9.5	0.126–0.248	940–4260
Glycerol 92%	1240	3270	62.5	2.5–6.4	2.5–8.6	0.455–0.729	1180–3500
Glycerol 99.5%	1260	12,500	62.0	2.4–6.4	2.3–8.6	1.74–2.90	1060–3450

†Air initially at 98.8 kPa and 297 ± 2 K. Properties of air taken at normal temperature and pressure: $\rho_c = 1.18$ kg/m^3, $\mu_c = 18.5 \times 10^{-6}$ kg/m s.

Table 3. Summary of liquid–liquid drop tower test conditions†

Dispersed phase	Water	Ethylene glycol	Glycerol 84%	Glycerol 99.5%	Carbon disulfide	DC200 fluid
Continuous phase	Paraffin oil	Paraffin oil	Paraffin oil	Paraffin oil	Water	Paraffin oil
ρ_d (kg/m^3)	997	1110	1219	1260	1263	970
ρ_c (kg/m^3)	870	870	870	870	997	870
$\mu_d \times 10^4$ (kg/ms)	8.9	145	632	12,500	6.5	300,000
$\mu_c \times 10^4$ (kg/ms)	710–1050	1050	1050	1050	8.9	1050
$\sigma \times 10^3$ (N/m)	46.8	39.0	39.5	32.1	45.6	22.0
d_o (mm)	6.8–58	4.0–31	5.2–7.3	6.0–22.5	1.8–5.6	0.1–0.6
We	0.2–20	0.1–7.4	0.5–2.0	0.5–24	0.2–3.5	0.004–0.06
Re	3.3–64	1.5–40	4.5–10	2.1–58	150–1190	0.03–0.75
Oh	$0.54–1.6 \times 10^{-3}$	$1.3–3.5 \times 10^{-2}$	0.16–0.20	1.3–2.5	$1.1–2.0 \times 10^{-3}$	77–215

†Liquids at 298 ± 3 K.

continuous phase included paraffin oil and water. Liquid properties were found as described in table 1, except that the properties of the paraffin oil also were obtained from the manufacturer. Initial drop diameters were in the range 0.1–58 mm while ranges of other variables were as follows: ρ_d/ρ_c of 1.15–1.45, Oh of 0.0005–215, We of 0.004–24 and Re of 0.03–1190. The We range was limited to conditions where interesting effects of deformation were observed but limited by the onset of breakup. The Re range extends from the Stokes regime to the region where the drag coefficient becomes relatively independent of Re (Faeth 1990; White 1974).

3. RESULTS AND DISCUSSION

3.1. Deformation and breakup regimes

Results for shock wave disturbances mainly involved extending the deformation and breakup regime map of Hsiang & Faeth (1992) to higher Oh, based on present results using the Dow Corning 200 Fluids. The resulting deformation and breakup regime map, showing transitions as functions of We and Oh similar to Hinze (1955) and Krzeczkowski (1980), is illustrated in figure 1. The experimental uncertainties (95% confidence) of present data values of We and Oh are less than 23 and 5%, respectively, due to the uncertainties of present drop diameter and velocity measurements. As noted in Hsiang & Faeth (1992), the various breakup regimes identified by Hinze (1955) and Krzeczkowski (1980), are in excellent agreement with the present measurements in the region where they overlap. This includes bag breakup at the onset of breakup, shear breakup that involves the stripping of liquid from the periphery of the drop, and the complex multimode breakup regime between them which merges aspects of the two bounding breakup regimes.

The transitions to the non-oscillatory and oscillatory deformation regimes illustrated in figure 1 have not been reported by others but are important because they define conditions where drop drag behavior departs significantly from that of a solid sphere. Thus, the first deformation regime involves the maximum (cross stream) dimension (normalized by the original drop diameter) in the range 1.05–1.10; with subsequent deformation regimes defined by this ratio being in the range 1.10–1.20 and greater than 1.20 but prior to transition to oscillatory deformation (at low Oh) or bag breakup (at large Oh). The oscillatory deformation regime is discussed in Hsiang & Faeth (1992): it is defined by conditions where the drop oscillated with a weakly damped amplitude (where the second peak of the drop diameter fluctuations exceeds a diameter ratio of 1.1).

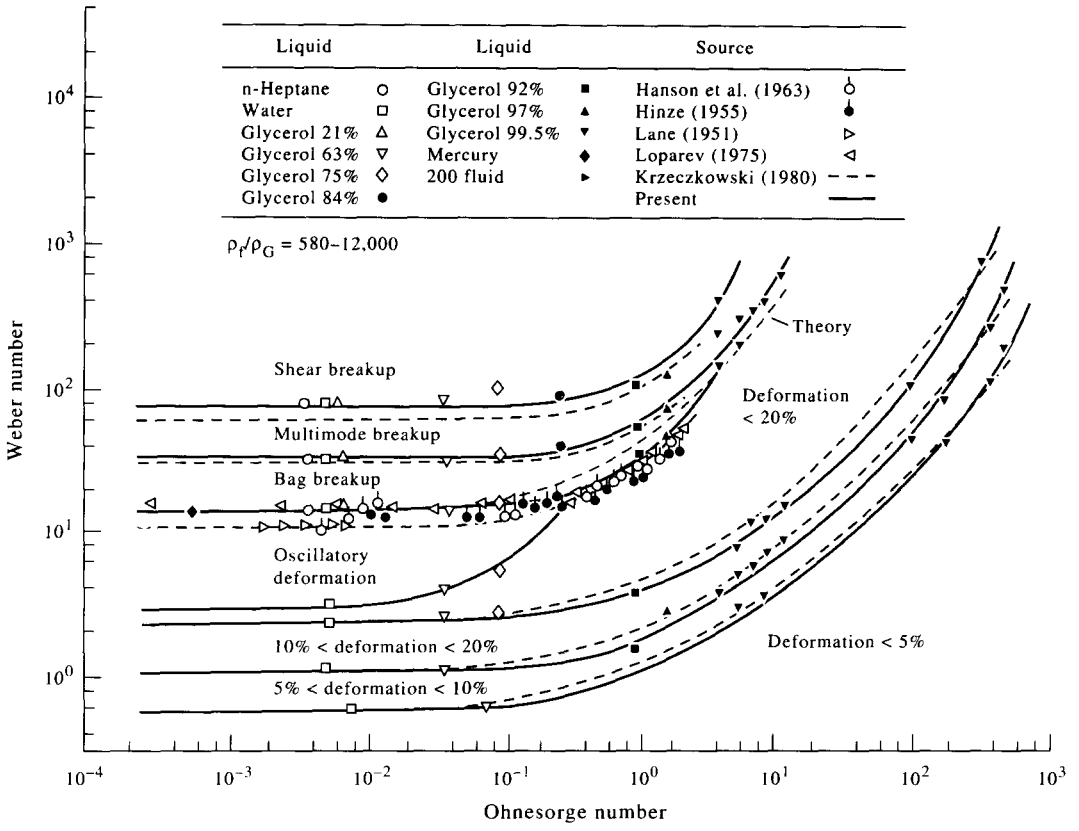

Figure 1. Drop deformation and breakup regime map for shock wave disturbances.

Perhaps the most striking feature of figure 1 is that while the We required for particular deformation and breakup regime transitions remain relatively constant for small Oh (values less that 0.1), the We required for the various transitions progressively increase with increasing Oh at large Oh (values greater than 1). Thus the onset of deformation (5–10% deformation) and breakup (bag breakup) occur at We of roughly 0.6 and 13 for $Oh < 0.1$; however, breakup no longer is observed for $We < 1000$ when $Oh > 10$ while deformation (5–10% deformation) disappears for a similar We range when $Oh > 1000$. Other deformation and breakup regimes observed at low Oh also disappear with increasing Oh, e.g. oscillatory deformation at Oh of roughly 0.3 and bag breakup at Oh of roughly 4. Hinze (1955) observed this tendency for the limited range of Oh available at the time ($Oh < 1$) and conjectured that breakup might no longer be observed for $Oh > 2$. However, the large Oh behavior observed in figure 1 does not suggest such a limitation; rather, there is a progressive (almost linear) increase of We at the deformation and breakup transitions, with increasing Oh. Clearly it is crucial to establish whether large Oh implies no deformation or breakup as suggested by Hinze (1955), or simply rather large values of We at the transitions, as suggested by the measurements illustrated, in figure 1. Thus, phenomenological analysis is considered next in order to gain more insight about effects of large Oh on deformation and breakup regime transitions.

Based on drop deformation results for steady disturbances, to be discussed subsequently, it did not appear that the liquid viscosity had a significant effect on the shape and hydrodynamic state of a deformed drop. Instead, the main effect of liquid viscosity for shock wave disturbances appeared to be reduction of the rate of deformation of the drop. This behavior allows more time for drop relaxation to the local ambient velocity, tending to reduce the relative velocity and thus the driving potential for drop deformation, at each stage of the deformation process. A simple analysis incorporating these ideas was carried out, in order to quantify the effect of liquid viscosity (represented by large Oh behavior) on deformation and breakup regime transitions.

The major assumptions of regime transition analysis were similar to earlier analysis of drop motion during breakup (Hsiang & Faeth 1992, 1993), as follows: virtual mass, Bassett history and

gravitational forces were ignored; gas velocities, and other properties, were assumed to be constant; drop mass was assumed to be constant; and a constant average drag coefficient was used over the period of interest. For present conditions, virtual mass and Bassett history forces are small because ρ_d/ρ_c is large (Faeth 1990). Similarly, gravitational forces are not a factor because drop motion was nearly horizontal and drag forces were much greater than gravitational forces. Additionally, uniform gas velocities, and other properties, were a condition of the experiments. Similarly, present considerations are limited to deformation and breakup regime transitions so that there is no mass loss of the drop. Finally, although drop drag coefficients vary considerably when drops are deformed, use of the original diameter and a constant average drag coefficient have been effective for earlier considerations of drop motion (Hsiang & Faeth 1993). Based on these assumptions, the equation governing the relative velocity, u, of the drop can be written as follows (Hsiang & Faeth 1993):

$$du/dt = -3\bar{C}_D\rho_c u^2/(4\rho_d d_o) \quad [1]$$

where the initial relative velocity is equal to u_o and $\bar{C}_D$ is an appropriate average drag coefficient. Now, previous results showed that the time required for breakup, etc., of large Oh drops could not be scaled systematically in terms of the characteristic low Oh breakup time, t^*, of Ranger & Nicholls (1969). Thus, the more appropriate characteristic time for large Oh conditions defined by Hinze (1948) was used instead as follows:

$$\tau = \mu_d/(\rho_c u_o^2) \quad [2]$$

Then, it was assumed that the maximum deformation condition, or the onset of breakup condition occurs at a time $t = K\tau$, where K is an empirical constant for the process being considered. Thus, completing the integration of [1] from $t = 0$ where $u = u_o$ to $t = K\tau$ where $u = u$, yields:

$$u_o/u = 1 + K'\mu_d/(\rho_d d_o u_o) \quad [3]$$

where

$$K' = 3\bar{C}_D K/4 \quad [4]$$

Using [3], the local Weber number of the drop can be expressed as follows:

$$\rho_c u^2 d_o/\sigma = \mathrm{We}/(1 + \mathrm{K'Oh}(\rho_c/\rho_d)^{1/2}/\mathrm{We}^{1/2})^2 \quad [5]$$

where $\mathrm{We} = \rho_c u_o^2 d_o/\sigma$ is the value based on initial conditions, as before. Then it was assumed that the local Weber number must reach a particular value, We_{cr}, for the regime transition of interest to occur. Finally, solving for the initial We to achieve the required We_{cr}, yields:

$$\mathrm{We} = (\mathrm{We}_{cr}/4)(1 + 4\mathrm{K'Oh}\mathrm{We}_{cr}^{-1/2}(\rho_c/\rho_d)^{1/2}) \quad [6]$$

Values of We_{cr} and K' were fitted to [6] to yield best-fit predicted transitions for the 5–10, 10–20 and 20% deformation regime transitions as well as the first breakup regime transition (typically for bag breakup). The resulting theoretical predictions of the regime transitions are illustrated in figure 1. In view of the simplifications of the theory, the agreement between predicted and measured regime transitions is seen to be reasonably good. Notably, [6] suggests that the transition We ~ Oh at large Oh rather than an ultimate limit for particular transitions at large Oh, as suggested by Hinze (1955). This is a very important difference in behavior that has significant relevance for processes of high pressure combustion, as noted earlier; therefore, this issue clearly merits additional study. In addition, whether present predictions of regime transitions apply for Oh and We > 1000 must still be established.

3.2. Dome/bowl transition

The present drop tower experiments were designed to define the properties of the deformed drop, and did not reveal strong effects of Oh over the available test range. Thus, a deformation and breakup regime map analogous to figure 1 for shock wave disturbances was not developed for steady disturbances (although effects of We on deformation for steady disturbances will be considered subsequently). However, a transition in drop shape, from dome- to bowl-shaped drops, was explored which will be discussed in the following.

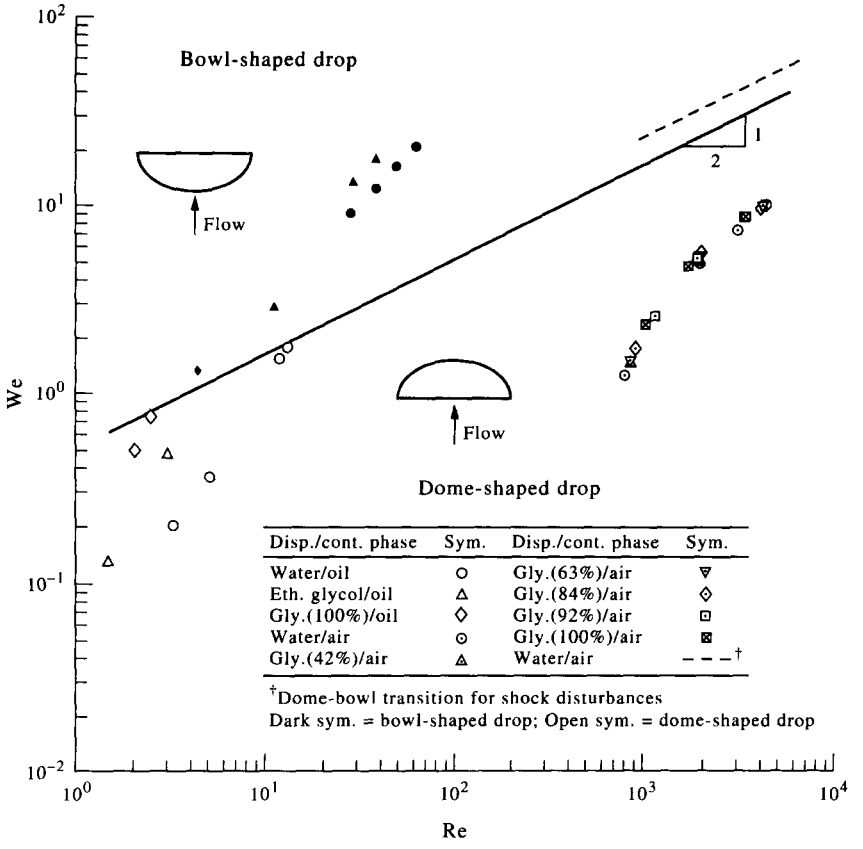

Figure 2. Dome- and bowl-shaped drop regime map.

Dome- and bowl-shaped drops are observed for both shock wave and steady disturbances. The general appearances of dome- and bowl-shaped drops are illustrated in figure 2. The windward or forward stagnation point side of a dome-shaped drop is flattened while the downstream side is rounded. This shape is similar to the appearance of a drop during bag breakup for shock wave disturbances, just at the start of the period where the bag begins to grow due to deformation of the center of the drop in a downstream direction (Hsiang & Faeth 1992). Thus, conditions for dome-shaped drops are somewhat analogous to conditions for bag breakup, and appear to involve interactions between drag and surface tension forces.

In contrast, for a bowl-shaped drop, as illustrated in figure 2, the forward stagnation region is rounded while the downstream side of the drop tends to be flattened, or even cup shaped in some instances. This shape is similar to the appearance of a drop during shear breakup for shock wave disturbances, just at the start of the period where drops are stripped from the periphery of the core (or drop forming) drop (Hsiang & Faeth 1993). Thus, conditions for bowl-shaped drops are somewhat analogous to conditions for shear breakup, and appear to involve interactions between drag and viscous forces.

The appearances of dome- and bowl-shaped drops suggest a simple means for establishing these regimes from the ratio of shear stresses to surface tension stresses. In doing this, shear stresses shall be estimated for the continuous phase, exploiting the fact that shear stresses are continuous at the drop surface, barring significant effects of surface tension gradients. Other major assumptions for these considerations are as follows: shear stresses are approximated by conditions for a laminar plane boundary layer, dispersed phase velocities are assumed to be small so that relative velocities are directly related to the velocity of the center of mass of the dispersed phase, and fluid properties are assumed to be constant. Then taking the length of the boundary layer to be proportional to the initial drop diameter, the characteristic shear stress, τ_w, becomes,

$$\tau_w = C\mu_c u_o/(\mu_c d/\rho_o u_o)^{1/2} \qquad [7]$$

where C is a constant of proportionality. The corresponding surface tension stress is proportional to σ/d_o assuming that d_o is a reasonable measure of the curvature of the drop surface. Equating these stresses then yields an expression for the transition Weber number between dome- and bowl-shaped drops, as follows:

$$We = C'Re^{1/2} \quad [8]$$

where C' is a constant of proportionality.

The dome- to bowl-shaped drop transition expression of [8] was evaluated using available data for both steady and shock wave disturbances. The results are plotted according to the variables of [8] in figure 2. The results for steady disturbances involve both liquid–liquid and liquid–gas systems, with experimental uncertainties (95% confidence) of present Re and We determinations less than 7 and 11%, respectively. The liquid–gas systems generally involve relatively large Re and relatively small We so that these conditions are well within the dome-shaped drop regime. Thus, the transition criterion illustrated in figure 2 was found using the liquid–liquid measurements, to yield the following correlation based on [8]

$$We = 0.5\ Re^{1/2}, \text{ steady disturbances} \quad [9]$$

Results for shock wave disturbances of drops in gases at low Oh also were considered. This transition was based on the observation that dome- and bowl-shaped drops are observed within the multimode breakup regime, near the end of the deformation period for values of We smaller and larger than roughly 40, respectively, This implies, for $Oh < 0.1$, the following relationship

$$We = 0.7\ Re^{1/2}, \text{ shock wave disturbances} \quad [10]$$

which has been entered on the plot as a dashed line.

In spite of the wide range of conditions, the different kinds of disturbances, and the different density ratios, the dome- to bowl-shaped drop transition illustrated in figure 2 is reasonably consistent with [8]. Furthermore, the transition over the present test range is reasonably expressed by either [9] or [10]. Perhaps this is not surprising; in fact, a number of investigators have suggested [8] as a criterion for the onset of shear breakup, as discussed by Borisov *et al.* (1981). However, it should be noted that this result generally pertains to conditions where Re is substantially greater than the Stokes regime (typically $Re > 10$). In contrast, other criteria known for the Stokes flow regime where a somewhat similar transition (from an oblate to a prolate spheroid) has been studied for some time, see Wellek *et al.* (1966), and references cited therein. Thus, more work is needed to reconcile these drop shape and breakup regime transitions within the Stokes and moderate Reynolds number regimes.

3.3. Drop deformation

Earlier work for shock wave disturbances found a relatively simple relationship between drop deformation and Weber number at small Oh (Hsiang & Faeth 1992). This result was based on phenomenological analysis of the interaction between surface tension and pressure forces when a drop is drawn into a flattened (oblate spheroid) shape due to relative motion of the continuous phase. The main assumptions of this analysis were as follows: the pressure difference between the bulk of the drop liquid and the continuous phase at the periphery of the drop is assumed to be proportional to the dynamic head of the flow, $\rho_c u^2/2$; this pressure difference is assumed to be stabilized by surface tension forces acting near the drop periphery; and the volume of the drop is assumed to be preserved, e.g. $d_{min} d_{max}^2 \sim d_o^3$. These ideas yielded the following expressions for the maximum and minimum dimensions of a drop, at the condition of maximum deformation for a shock wave disturbance, when Oh is small (Hsiang & Faeth 1992):

$$d_{max}/d_o = (d_{min}/d_o)^{-1/2} = 1 + C We^{1/2} \quad [11]$$

where C is an empirical constant, as before. During the present investigation, drop deformation measurements were summarized as d_{max}/d_{min}. Thus, based on [11] this ratio becomes:

$$d_{max}/d_{min} = (1 + C We^{1/2})^3 \quad [12]$$

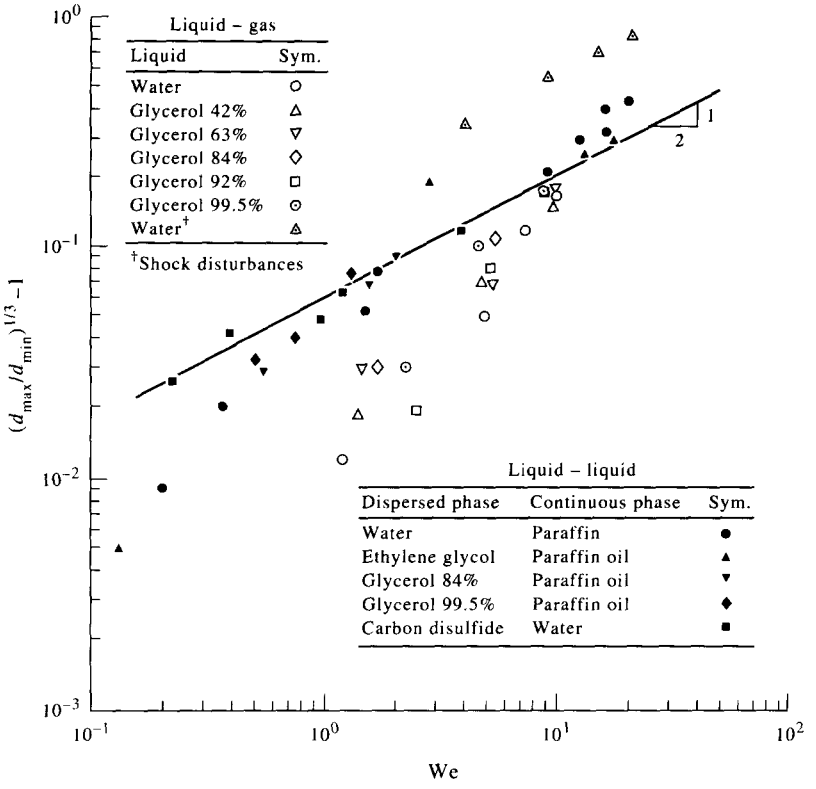

Figure 3. Drop deformation as a function of Weber number.

In view of earlier findings for deformation and breakup regime transitions for shock wave disturbances, it seemed reasonable that drop deformation for steady disturbances might satisfy an expression similar to [12] for both small and large Oh. In particular, the main effect of Oh for shock wave disturbances was to slow the rate of drop deformation so that local We at particular levels of deformation were reduced, rather than to modify the nature of the deformation at a particular local We condition. Thus, since drops have unlimited time to accommodate to a steady disturbance, it seems reasonable that the effect of Oh on deformation might be much reduced, as well.

Drop deformations for steady disturbances are plotted as suggested by [12] in figure 3. Results illustrated in the figure include drops at their terminal velocities in both gases and liquids. The experimental uncertainties (95% confidence) of the dependent variable is relatively large because the diameter ratio is near unity, e.g. on the order of 30 and 100% at values of the dependent variable of 0.1 and 0.03, respectively; the corresponding uncertainties of We are less than 11%. A representative result for water drops subjected to shock wave disturbances in air also is illustrated on the plot, where these results pertain to the maximum state of deformation of the drop during the period of interaction between the drop and the gas. A best-fit correlation of the steady disturbance measurements, according to [12] also is shown on the plot, as follows:

$$d_{max}/d_{min} = (1 + 0.07\ We^{1/2})^3 \qquad [13]$$

The measurements illustrated in figure 3 only are in fair agreement with the correlation of [13]. First of all, d_{max}/d_{min} for liquid–liquid systems are consistently larger than gas–liquid systems at a particular We. This behavior could be due to the effect of motion within the dispersed phase, which represents a larger fraction of the velocity difference between the dispersed and continuous phases for liquid–liquid than gas–liquid systems. In addition, significant circulatory motion within the dispersed phase would be expected to increase d_{max} due to centrifugal forces, as seen in the measurements of figure 3. Another deficiency of [13] is that the measurements decrease more rapidly as We decreases than is suggested by the correlation even though behavior at large We is represented reasonably well. This deficiency, however, is less significant because the discrepancies between the measurements and the correlation in this region are relatively small in comparison to

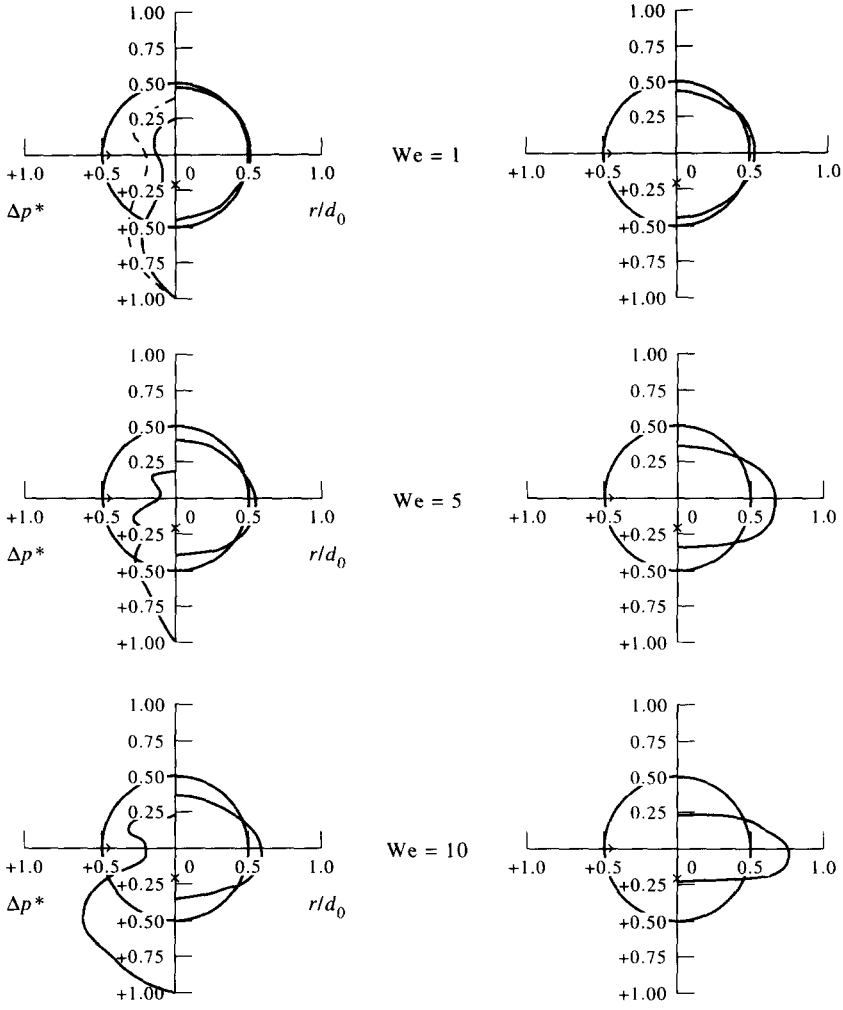

Figure 4. Drop shape and pressure distribution for steady (left-hand column) and shock wave (right-hand column) disturbances.

experimental uncertainties. Thus, [13] is provisional at best, pending more detailed measurements. Nevertheless, the measurements illustrated in figure 3 indicate that deformation mainly depends on We with density ratio, Oh and Re being secondary factors over the range of present measurements.

Comparing results for shock wave and steady disturbances in figure 3 shows that the maximum deformations for shock wave disturbances are greater than for steady disturbances at comparable conditions. This behavior is caused by inertial phenomena analogous to oscillatory deformation discussed in connection with figure 1. Thus, inertial effects cause the drop deformation to overshoot levels pertinent to steady disturbances at the same We.

The nature of overshoot effects on drop deformation is illustrated more thoroughly in figure 4. In this figure, drop shapes are plotted for We = 1, 5 and 10 for both steady (left hand column) and shock wave (right hand column) disturbances. As before, the shock wave disturbances pertain to the condition of maximum deformation of the drop for the indicated We. Additionally both sets of measurements are for liquid drops in gases. Finally, all the results illustrated in figure 4 are for We lower than required for the onset of secondary breakup, and are within the dome-shaped drop regime. The effect of overshoot is quite evident for the shock wave disturbances, which exhibit substantially larger maximum deformations than the steady disturbances at each value of We. Finally, the progressive increase of deformation with increasing We is very evident. This increased deformation provides a substantial increase of the drag forces acting on the drop due to the increased cross sectional area of the drop alone; furthermore, subsequent considerations will show

that drag coefficients are increased by deformation as well. Thus, drop deformation near the conditions for the onset of secondary breakup have a significant effect on drop dynamics.

3.4. *Drop drag*

The drop shape results for steady disturbances illustrated in figure 4 were used to obtain some insight about drop drag properties. This was done by estimating the static pressure, p, distribution around the drop, allowing for both hydrostatic and surface tension forces. The major assumptions of these calculations were as follows: effects of liquid motion within the drop were neglected, drops were assumed to be axisymmetric, effects of surface tension gradients were ignored and the hydrostatic pressure variation in the gas phase was neglected. The resulting static pressure estimates are plotted in figure 4 in terms of an effective pressure coefficient, defined as follows:

$$\Delta p^* = (1 + (p - p_\infty)/(\rho_c u_o^2/2))/2 \qquad [14]$$

where p_∞ is the static pressure far from the drop. The corresponding variation of Δp^* for flow over a solid sphere for a comparable Re range found from White (1974), also is illustrated in the figure for reference purposes (the dashed line illustrated for We = 1).

There are several interesting features about the static pressure distributions plotted in figure 4 for steady disturbances. First of all, Δp^* is unity at the forward stagnation point by definition. Secondly, static pressures decrease with increased angle from the forward stagnation point and tend to reach a minimum slightly before or near the 90° condition. Static pressures in the wake, however, do not recover to levels near the forward stagnation point because Re > 10 and the flow is separated in the wake region. This implies that 80–95% of the drag is due to form drag, caused by the static pressure distribution around the drop. Additionally, the increased drop deformation as We increases tends to increase the extent of the region of high static pressures near the forward stagnation point, which causes corresponding increases of the drag coefficient with deformation that will be discussed subsequently. Thus, while shear forces affect the mechanism of breakup of

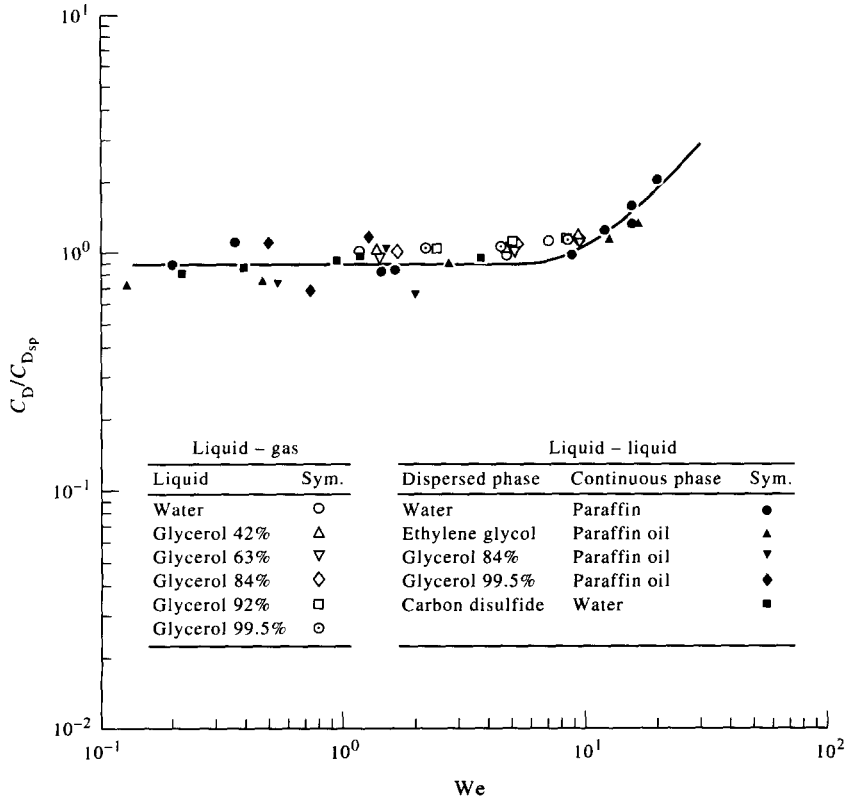

Figure 5. Drop drag coefficient as a function of deformation for steady disturbances.

the drop, as well as the transition between dome- and bowl-shaped drops, they really do not play a major role in the development of drop drag properties.

Drop drag coefficients, C_D, were defined in the usual manner, based on the maximum cross stream dimension of the drop and the relative velocity between the drop and continuous phases. The resulting drag coefficients for steady disturbances are plotted in figure 5. These results are plotted as C_D/C_{Dsp}, where C_{Dsp} is the drag coefficient of a sphere at the same Re, as a function of We. The experimental uncertainties (95% confidence) of the drag ratio are less than 10% while those for We are less than 11%. The values of We range from 0.1 to roughly 20, with the latter corresponding to maximum values of We without secondary breakup for steady disturbances. The measurements include results for drops in both gases and liquids.

Even though drops in gases exhibit a somewhat smaller deformation than drops in liquids at the same We, see figure 3, the results illustrated in figure 5 show that they generally have somewhat larger drag coefficients. In fact, drops in liquids have somewhat smaller drag coefficients than solid spheres for $We < 4$. This effect probably is due to motion of the drop liquid which is a larger fraction of the relative velocity for drops in liquids than drops in gases, e.g. the characteristic velocity for the drop phase is $(\rho_c/\rho_d)^{1/2}u$. Nevertheless, this reduction of the drag coefficient is not major in comparison to experimental uncertainties, e.g. C_D/C_{Dsp} is roughly 0.9 and 1.0 for $We < 4$ for drops in liquids and gases, respectively. Thus, it does not appear that density ratio has a significant effect on the drag coefficient for drops.

Considering all available data for the drag coefficients of drops in gases and liquids, and for shock wave and steady disturbances, it appears that C_D largely is a function of degree of deformation of the drop. This behavior is illustrated in figure 6, where present measurements of C_D for steady disturbances, and those of Hsiang & Faeth (1992) for shock wave disturbances, are plotted as a function d_{max}/d_{min}. The experimental uncertainties (95% confidence) of C_D for the steady disturbances are less than 10% while those for the shock wave disturbances are less than 30%. The corresponding uncertainties of the diameter ratio for steady and shock wave disturbances are less than 14 and 7%, respectively. It is evident that the results yield a single correlation with the main difference between the steady and shock wave disturbances being the larger range of d_{max}/d_{min} available prior to the onset of breakup for the latter. The range of the measurements is

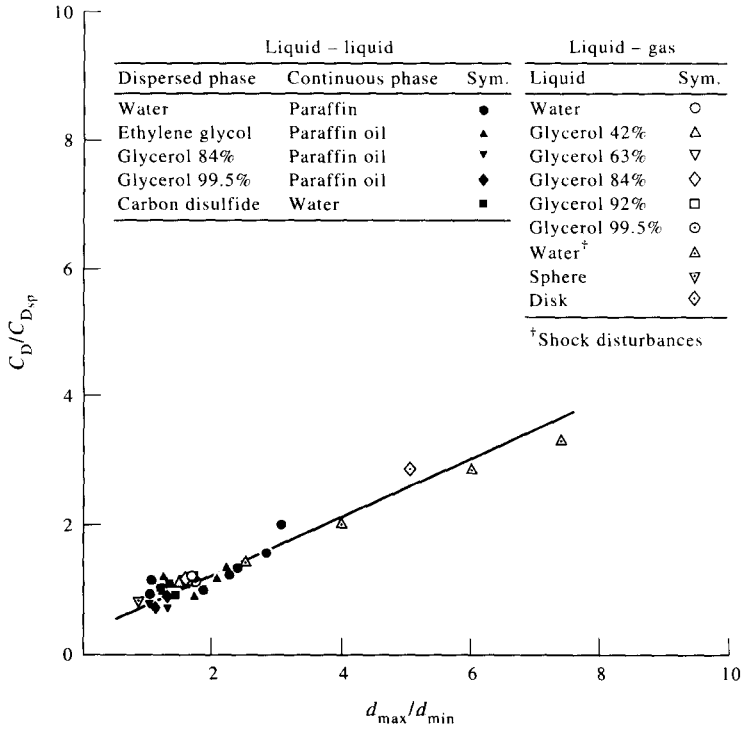

Figure 6. Drop drag coefficient as a function of deformation for both shock wave and steady disturbances.

C_D/C_{Dsp} of 1.0–3.5 for d_{max}/d_{min} of 1.0–7.5. Thus there is roughly a 3:1 increase of drag coefficient in going from a round drop to a highly deformed and flattened drop, which is reasonable because the change is comparable to the change of C_D between a round sphere and a thin disk (White 1974). This behavior, combined with the increased cross-sectional area of the drop, causes a substantial increase in the drag forces acting on deformed drops in comparison to the original undeformed drop. For example, the ratio of the drag forces is $(d_{max}/d_o)^2(C_D/C_{Dsp})$ which becomes $(d_{max}/d_{min})^{2/3}(C_D/C_{Dsp})$ from [11] and [12]. Applying this equation to the results illustrated in figure 6 then yields deformed/non-deformed drag force ratios of roughly 4 and 13 for drops having maximum deformations for steady and shock wave disturbances, respectively.

4. CONCLUSIONS

Drop deformation and breakup for both shock wave and steady disturbances were studied. Several liquids were considered for the dispersed (drop) phase, including water, *n*-heptane, mercury, Dow Corning 200 Fluids, various glycerol mixtures, ethylene glycol and carbon disulfide. Continuous phases included air, paraffin oil and water. Overall test conditions involved ρ_d/ρ_c of 1.15–12,000, Oh of 0.0005–600, We of 0.004–700 and of 0.03–16,000. The major conclusions of the study are as follows:

(1) For shock wave disturbances at small Oh (Oh < 0.1), significant drop deformation (5–10% deformation regime) was observed at We of roughly 0.6 while bag, multimode and shear breakup began at We = 13, 35 and 80, respectively.

(2) For shock wave disturbances at large Oh (Oh > 1) the critical We for the onset of various deformation and breakup regimes became roughly proportional to Oh, which could be attributed to increased resistance of drops to deformation at large Oh, based on phenomenological analysis (note that behavior for Oh and We > 1000 still must be studied, however). In addition, the oscillatory deformation and the bag breakup regimes disappeared with increasing Oh, at Oh = 0.3 and 4, respectively.

(3) An important transition from dome- to bowl-shaped drops (which is related to the transition between bag and shear breakup) appears to be controlled by $We/Re^{1/2}$ for the present Re range, but other criteria known for analogous transitions in the Stokes flow regimes must still be reconciled with this behavior.

(4) Drop deformation for steady disturbances mainly varied with We, while minor effects of ρ_d/ρ_c on deformation mainly were attributed to corresponding variations of Re. Thus, the main effect of increased drop viscosity (represented by Oh) on drop deformation and breakup for general disturbances is to reduce rates of drop distortion so that drop relaxation reduces relative velocities when the maximum deformation is reached, and thus the propensity for drop deformation and breakup.

(5) Drop drag coefficient ratios, C_D/C_{Dsp}, were relatively independent of the type of disturbance, ρ_d/ρ_c We, Oh and Re; instead, these ratios correlated mainly with drop deformation, while evolving from values near unity for small distortions to values typical of thin disks for large distortions. This increase in C_D and the corresponding increase of the cross-sectional area of the drop, due to distortion, causes drag forces to increase by factors of roughly 4 and 13 at deformation conditions typical of the onset of breakup for steady and shock wave disturbances, respectively, which clearly has an important impact on breakup dynamics.

Acknowledgements—This research was sponsored by the Air Force Office of Scientific Research, Grant No. F49620-92-J-0399, under the technical management of J. N. Tishkoff. The authors would like to thank C. W. Kauffman for the loan of the shock tube facility and advice concerning its operation. The U.S. Government is authorized to reproduce and distribute copies for governmental purposes notwithstanding any copyright notation thereon.

REFERENCES

Borisov, A. A., Gel'fand, B. E., Natanzon, M. S. & Kossov, O. M. 1981 Droplet breakup regimes and criteria for their existence. *Inzh.-Fizich. Zl* **40,** 64–70.

Clift, R. Grace, J. R. & Weber, M. E. 1978 *Bubbles, Drops and Particles*, pp. 26 and 339–347. Academic Press, New York.

Dabora, E. K. 1967 Production of monodisperse sprays. *Rev. Scient. Instrum.* **38,** 502–506.

Faeth, G. M. 1990 Structure and atomization properties of dense turbulent sprays. In *Twenty-Third Symposium (International) on Combustion*, The Combustion Institute, Pittsburgh, pp. 1345–1352.

Gel'fand, B. E., Gubin, S. A. & Kogarko, S. M. 1974 Various forms of drop fractionation in shock waves and their special characteristics. *Inzh.-Fizich. Zl* **27,** 119–126.

Giffen, E. & Muraszew, A. 1953 *The Atomization of Liquid Fuels*. Wiley, New York.

Hanson, A. R., Domich, E. G. & Adams, H. S. 1963 Shock-tube investigation of the breakup of drops by air blasts. *Phys. Fluids* **6,** 1070–1080.

Hinze, J. O. 1948 Critical speeds and sizes of liquid globules. *Appl. Sci. Res.* **11,** 273–287.

Hinze, J. O. 1955 Fundamentals of the hydrodynamic mechanism of splitting in dispersion processes. *AIChE Jl* **1,** 289–295.

Hsiang, L.-P. & Faeth, G. M. 1992 Near-limit drop deformation and secondary breakup. *Int. J. Multiphase Flow* **18,** 635–652.

Hsiang, L.-P. & Faeth, G. M. 1993 Drop properties after secondary breakup. *Int. J. Multiphase Flow* **19,** 721–735.

Krzeczkowski, S. A. 1980 Measurement of liquid droplet disintegration mechanisms. *Int. J. Multiphase Flow* **6,** 227–239.

Lane, W. R. 1951 Shatter of drops in streams of air. *Ind. Engng Chem.* **43,** 1312–1317.

Lange, N. A. 1952 *Handbook of Chemistry*, 8th edn, pp. 1134 and 1709. Handbook Publishers Inc., Sandusky, OH.

Liang, P. Y., Eastes, T. W. & Gharakhari, A. 1988 Computer simulations of drop deformation and drop breakup. AIAA Paper No. 88-3142.

Loparev, V. P. 1975 Experimental investigation of the atomization of drops of liquid under conditions of a gradual rise of the external forces. *Izvestiya Akad. Nauk SSSR, Mekh. Zhidkosti Gaza* **3,** 174–178.

Pruppacher, H. R. & Pitter, R. L. 1971 A semi-empirical determination of the shape of cloud and rain drops. *J. Atmos. Sci.* **28,** 86–94.

Ranger, A. A. & Nicholls, J. A. 1969 The aerodynamic shattering of liquid drops. *AIAA Jl* **7,** 285–290.

Reinecke, W. G. & McKay, W. L. 1969 Experiments on waterdrop breakup behind Mach 3 to 12 shocks. Sandia Corp. Report SC-CR-70-6063.

Reinecke, W. G. & Waldman, G. D. 1970 A study of drop breakup behind strong shocks with applications to flight. Avco Report AVSD-0110-70-77.

Ruff, G. A., Wu, P.-K., Bernal, L. P. & Faeth, G. M. 1992 Continuous- and dispersed-phase structure of dense non-evaporating pressure-atomized sprays. *J. Prop. Power* **8,** 280–289.

Ryan, R. T. 1976 The behavior of large low-surface-tension water drops falling at terminal velocity in air. *J. Appl. Meteorol.* **15,** 157–165.

Sangiovanni, J. & Kestin, A. S. 1977 A theoretical and experimental investigation of the ignition of fuel droplets. *Combust. Sci. Technol.* **6,** 59–70.

Simmons H. C. 1977 The correlation of drop-size distributions in fuel nozzle sprays. *J. Engng Power* **99,** 309–319.

Wellek, R. M., Agrawal, A. K. & Skelland, A. H. P. 1966 Shape of liquid drops moving in liquid media. *AIChE Jl 12*, 854–862.

White, F. M. 1974 *Viscous Fluid Flow*. McGraw-Hill, New York.

Wierzba, A. & Takayama, K. 1987 Experimental investigations on liquid droplet breakup in a gas stream. Rep. Inst. High Speed Mech., Tohoku Univ., Vol. 53, No. 382, pp. 1–99.

Wu, P.-K., Ruff, G, A. & Faeth, G. M. 1991 Primary breakup in liquid/gas mixing layers. *Atom. Sprays* **1,** 421–440.

Wu, P.-K., Tseng, L.-K. & Faeth, G. M. 1992 Primary breakup in gas/liquid mixing layers for turbulent liquids. *Atom. Sprays* **2,** 295–317.